Broad near-ultraviolet and blue excitation band induced dazzling red emissions in Eu³⁺-activated Gd₂MoO₆ phosphors for white light-emitting diodes†

Peng Du,[a] Yue Guo,[b] Soo Hyun Lee[a] and Jae Su Yu*[a]

A series of Eu³⁺-activated Gd₂MoO₆ phosphors were synthesized *via* a citric acid-assisted sol–gel route. The photoluminescence (PL) excitation spectra revealed that the obtained phosphors can be efficiently pumped by both near-ultraviolet and blue light. Upon 360 and 463 nm excitation, bright emissions corresponding to the $^5D_0 \rightarrow {}^7F_J$ (J = 0, 1, 2, 3 and 4) transitions of Eu³⁺ ions were detected. Meanwhile, the PL emission intensity was strongly dependent on the Eu³⁺ ion concentration and the optimal doping concentration for the Eu³⁺ ions in the Gd₂MoO₆ host lattice was determined to be around 15 mol%. The critical distance was around 11.47 Å and the mechanism for the concentration quenching was dominated by dipole–dipole interaction. Furthermore, the temperature-dependent PL emission spectra were recorded to test the thermal stability of the as-synthesized phosphors. Additionally, the Judd–Ofelt theory was employed to investigate the local crystal environment around the Eu³⁺ ions in the Eu³⁺-activated Gd₂MoO₆ phosphors. Finally, by integrating the resultant compounds with a blue light-emitting diode (LED) chip and yellow-emitting YAG:Ce³⁺ phosphors, a white light-emitting diode (WLED) device was fabricated which possessed a correlated color temperature of 5981 K, a color rendering index of 71.76 and a color coordinate of (0.321, 0.378). The results suggest that the Eu³⁺-activated Gd₂MoO₆ compounds are a promising red-emitting phosphor for WLEDs.

1. Introduction

Over the last few years, considerable efforts have been dedicated to the development of rare-earth (RE) ion-based luminescent materials because of their extensive practicability in various fields, including solar cells, optical bioimaging, noninvasive temperature sensors, latent fingerprinting, white light-emitting diodes (WLEDs) and solid-state lasers.[1–9] In particular, with the growing awareness of environmental problems and energy consumption, the investigation of phosphor-converted WLEDs is increasing since their utilization can save around 50% of the energy for lighting and they are eco-friendly compared to conventional bulbs.[10] At present, the combination of a blue LED chip and yellow-emitting YAG:Ce³⁺ phosphors is a commercially available strategy to generate white light. Unfortunately, due to the deficiency of red emission band in the luminescent spectrum, the white light usually suffers high correlated color

temperature (CCT) and low color rendering index (CRI).[11,12] To circumvent these shortages, another feasible approach was developed, that is, using the ultraviolet (UV) or near-UV (NUV) LED chip to pump the blending tricolor (blue, green and red) phosphors to produce the warm white light.[13–16] Obviously, the red-emitting phosphor is an indispensable component for the generation of high-quality white light. Up to now, some red-emitting phosphors, such as Y₂O₂S:Eu³⁺,[17] CaZnS:Eu²⁺,[18] Sr₂Si₅N₈:Eu²⁺,[19] and Sr[LiAl₃N₄]:Eu²⁺,[20] have been created for WLEDs. However, these compounds usually exhibit poor stability and need some rigorous reaction conditions. Meanwhile, these red-emitting phosphors can only be efficiently excited either by NUV or blue light. Considering these issues, searching for a novel red-emitting phosphor, which can be simultaneously pumped by NUV and blue light, with high stability, low cost and satisfactory luminescent performance is required.

Eu³⁺ ion is known to be a red-emitting activator as a result of its predominant $^5D_0 \rightarrow {}^7F_2$ transition at around 610 nm.[21,22] It was reported that bright red emissions originating from the 4f–4f transition of Eu³⁺ ions were achieved in some Eu³⁺-activated inorganic host lattices, such as tungstates, borates, phosphates, molybdates and vanadates.[23–27] In comparison with other inorganics, the molybdate compounds acting as the

aDepartment of Electronics and Radio Engineering, Kyung Hee University, Yongin-si, Gyeonggi-do 446-701, Republic of Korea. E-mail: jsyu@khu.ac.kr; Fax: +82 31 201 3820; Tel: +82 31 206 2820

bDepartment of Physics, Pukyong National University, Busan 608-737, Republic of Korea

† Electronic supplementary information (ESI) available. See DOI: 10.1039/c6ra25652j

luminescent host lattices have attracted much attention due to their merits of superior inherent luminescent properties and high stability. Furthermore, the molybdates with the octahedral MoO_6 groups were found to have a strong broad charge transfer (CT) band (~250–450 nm) corresponding to the $O^{2-} \rightarrow Mo^{6+}$ transition.[28,29] Consequently, the RE ions-based molybdate compounds are presumed to exhibit high-efficiency luminescent properties. Zou *et al.* demonstrated that the Eu^{3+}-activated Bi_2MoO_6 phosphors could emit bright red emissions under UV light excitation.[30] It was also revealed that the Ba_2ZnMoO_6:Eu^{3+} phosphors were suited for WLEDs as red-emitting phosphors.[31] Although some splendid performances have been gained in the RE ions activated molybdate phosphors, to extend their vivid applications in solid-state lighting, more endeavors should be made to further improve their luminescent properties. In this work, the Gd_2MoO_6, which possesses a monoclinic scheelite structure with cell parameters of $a = 15.67$ Å, $b = 11.16$ Å, $c = 5.419$ Å and $V = 947.65$ Å^3, was selected as the luminescent host lattice. The conventional sol–gel method was applied to prepare the Eu^{3+}-activated Gd_2MoO_6 red-emitting phosphors. The phase structure, morphological performance, thermal stability and luminescent properties of the resultant products were systematically studied. It is worth noting that the synthesized phosphors can be efficiently excited by both NUV and blue light which was superior to those of the previously developed red-emitting phosphors. In addition, to identify the symmetry property of the dopants in the Gd_2MoO_6 host lattice, the Judd–Ofelt (J–O) theory was employed to estimate the J–O intensity parameters. Ultimately, a WLED device was fabricated by using the blue LED chip to pump the blended yellow-emitting YAG:Ce^{3+} and formed red-emitting phosphors to examine the potentiality of the Eu^{3+}-activated Gd_2MoO_6 phosphors for WLEDs.

2. Experimental

2.1 Synthesis of Eu^{3+}-activated Gd_2MoO_6 phosphors

A series of $Gd_{2-2x}MoO_6$:$2x$Eu^{3+} (Gd_2MoO_6:$2x$Eu^{3+}; $x = 0.01$, 0.05, 0.10, 0.15, 0.20 and 0.30) were synthesized by a facile citrate-assisted sol–gel technique. The ammonium molybdate tetrahydrate ($(NH_4)_6Mo_7O_{24} \cdot 4H_2O$; 99%), gadolinium nitrate hexahydrate ($Gd(NO_3)_3 \cdot 6H_2O$; 99.9%), citric acid ($HOC(COOH) \cdot (CH_2COOH)_2$; 99.5%) and europium nitrate pentahydrate ($Eu(NO_3)_3 \cdot 5H_2O$; 99.9%) purchased from Sigma were used as the raw materials. The stoichiometric amounts of $Gd(NO_3)_3 \cdot 6H_2O$, $(NH_4)_6Mo_7O_{24} \cdot 4H_2O$ and $Eu(NO_3)_3 \cdot 5H_2O$ were weighted and dissolved in 200 ml of deionized water. After stirring 20 min with the help of magnetic stirrer, a transparent solution was achieved. Subsequently, the citric acid acting as the chelating agent was added into the above solution (with the molar ratio of citric acid to metal ions of 2 : 1). Then, the beaker was covered with a lid and heated at 80 °C for 3 h under strong mechanical agitation. After that, the lid of the beaker was removed and the solution was evaporated gradually to form a wet-gel. The wet-gel was shifted to the oven and dried at 120 °C for 12 h, and the xerogel was gained. Ultimately, the resultant xerogel was kept in the furnace and calcined at 1100 °C for 6 h with

the heating ratio of 5 °C min^{-1} to obtain the Eu^{3+}-activated Gd_2MoO_6 phosphors.

2.2 Characterization

The crystallinity and phase composition of the formed compounds were checked by a X-ray diffractometer (Bruker D8 Advance) with Cu Kα radiation. The microstructure and composition of the resultant samples were identified by the field-emission scanning electron microscope (FE-SEM) (LEO SUPRA 55, Carl Zeiss) and transmission electron microscope (TEM) (JEM-2100F, JEOL) equipped with an energy-dispersive X-ray spectroscopy (EDS). The spectrofluorometer (Scinco FlurO-Mate FS-2) equipped with a xenon lamp as the light source was applied to examine the luminescent properties of the as-prepared phosphors. The temperature-dependent PL emission spectra of the synthesized products were recorded by the FS-2 system to explore their thermal stability and the temperature from 303 to 483 K was controlled by a temperature controlled stage (NOVA ST540). Under different excitation wavelengths, the absolute quantum efficiency of the studied samples was measured by a fluorescence spectrophotometer equipped with integrating sphere (Hamamatsu Photonics C9920-02). The electroluminescence (EL) spectra of the fabricated LED devices were measured by a multi-channel spectroradiometer (OL 770) under a forward bias current of 50 mA.

3. Results and discussion

3.1 Phase identification and morphology

The phase composition of the Eu^{3+}-activated Gd_2MoO_6 phosphors which were synthesized by a facile citric acid assisted sol–gel method was analyzed by X-ray diffraction (XRD). From the XRD patterns, as displayed in Fig. 1, it is clear that all the diffraction peaks of the studied samples were well indexed to the standard Gd_2MoO_6 with a space group of $I2/a(15)$ (JCPDS#
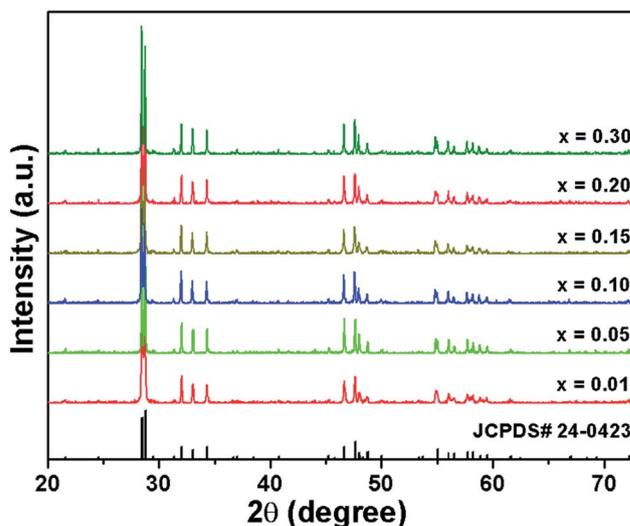

Fig. 1 XRD patterns of Gd_2MoO_6:$2x$Eu^{3+} ($x = 0.01$, 0.05, 0.10, 0.15, 0.20 and 0.30) phosphors calcined at 1100 °C.

24-0423). The result confirmed that all the compounds possessed pure monoclinic phase and the introduction of Eu^{3+} ions into the Gd_2MoO_6 host lattice had little impact on the crystal structure. Considering the ionic radius and charge balance of the existing cations, the dopants (Eu^{3+}) were preferred to occupy the sites of Gd^{3+} ions in Gd_2MoO_6. On the basis of previous reports, the radius percentage difference (D_r) between the dopants and the possible substituted ions is defined as:[3,11]

$$D_r = \frac{R_s(CN) - R_d(CN)}{R_s(CN)} \times 100\%, \tag{1}$$

where $R_s(CN)$ and $R_d(CN)$ stand for the ionic radii of substituted ions and dopants, respectively. Generally, to form a new solid solution, the D_r value should be below 15%.[3,32] In present work, the ionic radii for the Gd^{3+} and Eu^{3+} ions were around 1.053 and 1.066 Å, respectively, when the coordinate number (CN) was 8. Thus, the D_r value for Eu^{3+}/Gd^{3+} was estimated to be about -1.23%. Since the calculated D_r value was much smaller than 15%, the Gd^{3+} ions could be easily taken place by Eu^{3+} ions without inducing any distinct changes to the structure of the Gd_2MoO_6 host lattice.

To further confirm the Eu^{3+} ions preferred to inhabit the sites of Gd^{3+} ions in Gd_2MoO_6, the Rietveld refinement based on the XRD pattern of the Gd_2MoO_6:0.30Eu^{3+} phosphors was performed with the help of General Structure Analysis System and the corresponding fitting pattern is displayed in Fig. 2. The final refined lattice parameters as well as the reliability factors are summarized in Table S1.† As presented in Table S1,† the reliability factors were $R_p = 5.31\%$, $R_{wp} = 4.22\%$ and $\chi^2 = 1.47$. Meanwhile, the lattice constants of Gd_2MoO_6:0.30Eu^{3+} phosphors were found to be $a = 15.68645$ Å, $b = 11.18177$ Å, $c = 5.41992$ Å and $V = 950.55$ Å^3 (see Table S1†). Note that, these calculated cell constants were slightly larger than those of pure Gd_2MoO_6 ($a = 15.67$ Å, $b = 11.16$ Å, $c = 5.419$ Å and $V = 947.65$ Å^3; JCPDS# 24-0423), further revealing that the Eu^{3+} ions can be

doped into the Gd_2MoO_6 host lattice by replacing the Gd^{3+} ions and did not cause any obvious variations to the host crystal structure matched well with the above discussion. By means of the Diamond software, the unit cell structure of Gd_2MoO_6 was modeled, as illustrated in the inset of Fig. 2. It is evident that the Gd^{3+} ions were coordinated by eight oxygen atoms while the Mo^{6+} ions were surrounded by four oxygen atoms.

The crystallinity and microstructure features of Eu^{3+}-activated Gd_2MoO_6 phosphors were characterized by FE-SEM and TEM. Fig. 3 depicts the representative FE-SEM and TEM images of the Gd_2MoO_6:0.30Eu^{3+} phosphors. Both the FE-SEM and TEM image revealed that the synthesized compounds were made up of irregular particles with the size ranging from approximately 300 to 600 nm (see Fig. 3(a) and (b)). As demonstrated in Fig. 3(c), the high-resolution TEM (HR-TEM) image showed distinct lattice fringes with the d-spacing of around 3.08 Å which was in good agreement with the distance of (321) plane for Gd_2MoO_6. The selected area electron diffraction (SAED) pattern, as shown in Fig. 3(d), exhibited bright dot patterns, illustrating that the single nanocrystalline nature of the obtained particles. The EDS spectrum, which was taken from the TEM image (Fig. 4(a)), was employed to detect the element constitution of the Gd_2MoO_6:0.30Eu^{3+} phosphors, as depicted in Fig. 4(b). The observed peaks of Gd, Mo, O and Eu in the EDS spectrum further confirmed the formation of Eu^{3+}-activated Gd_2MoO_6 phosphors. Meanwhile, the elemental mapping result also indicated that the Gd, Mo, O and Eu were equally distributed in the range of the nanoparticles (see Fig. 4(c)–(f)).

3.2 Room-temperature luminescent behavior

The typical PL excitation (PLE) spectrum of the Gd_2MoO_6:0.30-Eu^{3+} phosphors, which was recorded at the dominant red emission wavelength (610 nm) of Eu^{3+} ions, is shown in Fig. 5(a). As described in Fig. 5(a), the PLE spectrum contained
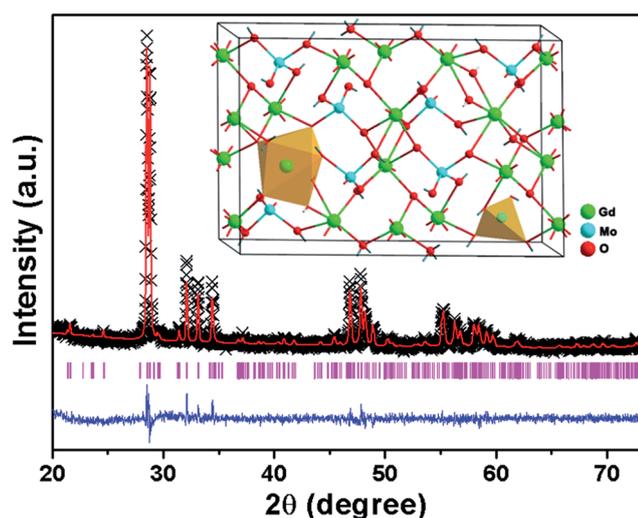

Fig. 2 Rietveld XRD refinement for the Gd_2MoO_6:0.30Eu^{3+} phosphors. Inset shows the unit cell structure of the Gd_2MoO_6.

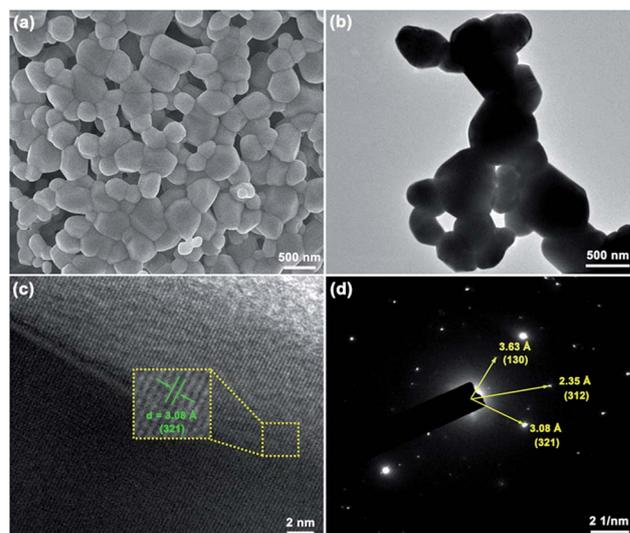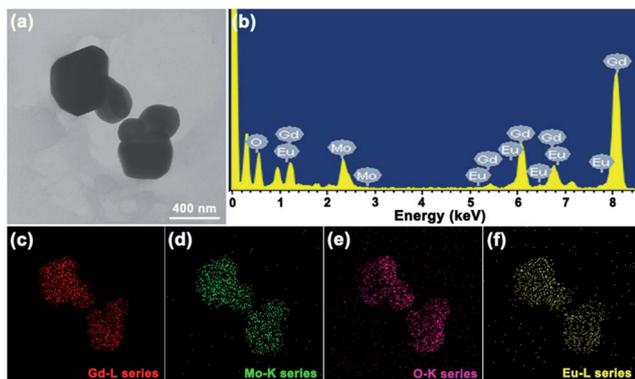**Fig. 3** (a) FE-SEM image, (b) TEM image, (c) HR-TEM image and (d) SAED pattern of the Gd_2MoO_6:0.30Eu^{3+} phosphor.

Fig. 4 (a) TEM image, (b) EDS spectrum and (c, d, e and f) elemental mappings of the $Gd_2MoO_6:0.30Eu^{3+}$ phosphors.

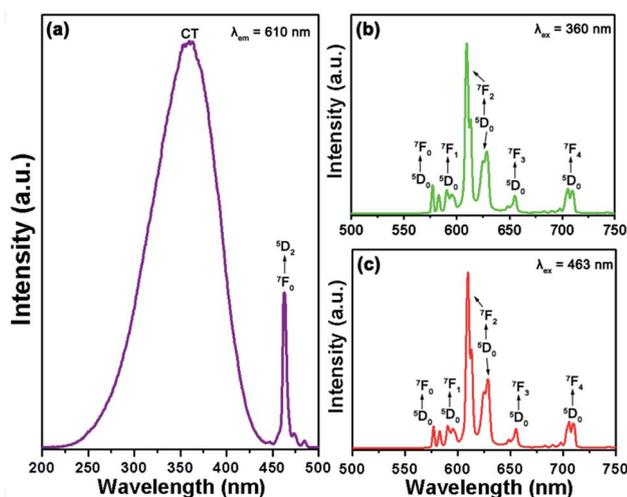Fig. 5 (a) PLE spectrum of the $Gd_2MoO_6:0.30Eu^{3+}$ phosphors monitored at 610 nm. (b and c) PL emission spectra of the $Gd_2MoO_6:0.30Eu^{3+}$ phosphors excited at 360 and 463 nm, respectively.

a broad band and a sharp peak. The broad band of 225–450 nm centered at around 360 nm is called as charge transfer (CT) band which is ascribed to the overlap transitions of $O^{2-} \rightarrow Mo^{6+}$ and $O^{2-} \rightarrow Eu^{3+}$.[33,34] The narrow excitation band located at approximately 463 nm occurred from the $^7F_0 \rightarrow {}^5D_2$ transition of Eu^{3+} ions.[35] With the increase of Eu^{3+} ion concentration, the PLE spectra did not show a significant change, while the intensity of the excitation peaks was increased and its maximum value was achieved when the doping concentration was 15 mol% (see Fig. S1†). These results clearly indicated that the as-prepared phosphors can be simultaneously excited by both NUV and blue light. Upon 360 nm excitation, the PL emission spectrum of the $Gd_2MoO_6:0.30Eu^{3+}$ phosphors was measured as presented in Fig. 5(b). Clearly, the PL emission spectrum was dominated by a strong red emission with a center of about 610 nm due to the $^5D_0 \rightarrow {}^7F_2$ transition.[36] Meanwhile, there also existed some relatively weak excitation peaks at 577, 589, 655 and 705 nm which are attributed to the 4f–4f transitions of Eu^{3+} ions from the excited state of $^5D_0$ to $^7F_0$, $^7F_1$, $^7F_3$

and $^7F_4$, respectively.[37] On the basis of previous works,[38,39] one knows that the Eu^{3+}-activated luminescent materials usually exhibit two characteristic emissions in the yellow ($^5D_0 \rightarrow {}^7F_1$) and red ($^5D_0 \rightarrow {}^7F_2$) regions. Especially, according to the magnetic dipole (MD) transition rule ($\Delta J = 0, \pm 1$), the $^5D_0 \rightarrow {}^7F_1$ ($\Delta J = 1$) transition belongs to the MD transition, whereas the $^5D_0 \rightarrow {}^7F_2$ transition pertains to the hypersensitive electric dipole (ED) transition which is sensitive to its surrounding crystal field.[40,41] Normally, the red emission ($^5D_0 \rightarrow {}^7F_2$) takes the domination in the PL emission spectrum when the Eu^{3+} ions occupy the sites without inversion centers. In present work, in comparison with that of the $^5D_0 \rightarrow {}^7F_1$ transition, the emission intensity of the $^5D_0 \rightarrow {}^7F_2$ transition was much stronger (see Fig. 5(b)), demonstrating that the Eu^{3+} ions occupied the low symmetry sites with non-inversion centers in Gd_2MoO_6 host lattice. Meanwhile, under the excitation of 463 nm, the $Gd_2MoO_6:0.30Eu^{3+}$ phosphors exhibited the characteristic emissions of Eu^{3+} ions and the PL emission spectral profile was the same as that under the excitation of 360 nm, as displayed in Fig. 5(b) and (c), further revealing that the Eu^{3+}-activated Gd_2MoO_6 phosphors could be efficiently pumped by both the NUV and blue light, which coincided well with previous discussion. Fig. 6 illustrates the energy level scheme of Eu^{3+} ions in Gd_2MoO_6 host lattice to expound the involved luminescent processes.

As we know, the doping concentration has an obvious influence on the PL emission intensity of the RE ions activated luminescent materials. For the sake of achieving the optimum doping concentration of Eu^{3+} ions in Gd_2MoO_6, a series of $Gd_2MoO_6:2xEu^{3+}$ phosphors were fabricated via a conventional sol–gel method and their luminescent properties were examined. The PL emission spectra of $Gd_2MoO_6:2xEu^{3+}$ phosphors, which were excited at 360 and 463 nm, are shown in Fig. 7 and S2,† respectively. It is evident that the featured emissions of Eu^{3+} ions were observed in all the obtained compounds and the PL emission spectral profiles were almost the same, while the PL emission intensity varied with raising the Eu^{3+} ion

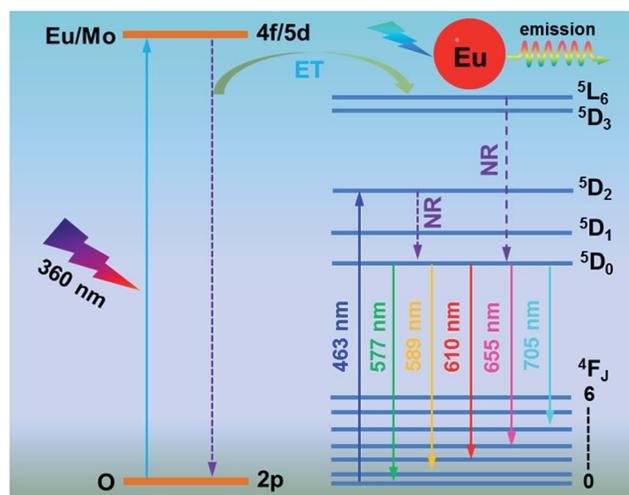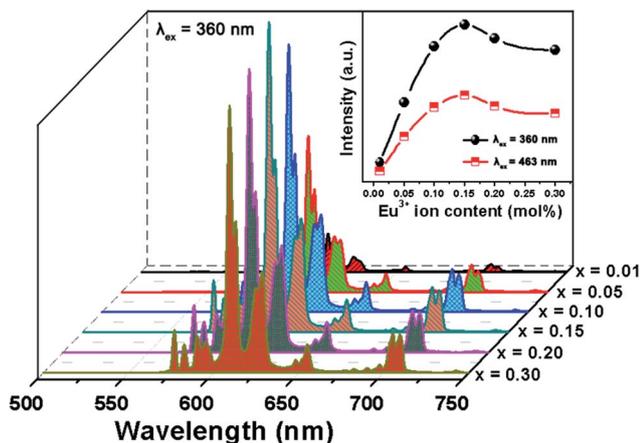Fig. 6 Energy level diagram of Eu^{3+} ions along with the possible luminescent routes in Eu^{3+}-activated Gd_2MoO_6 phosphors.

Fig. 7 PL emission spectra of $Gd_2MoO_6:2xEu^{3+}$ phosphors upon the excitation of 360 nm. Inset presents the PL emission intensity as a function of Eu^{3+} ion concentration excited at 360 and 463 nm.

concentration (see Fig. 7 and S2†). As demonstrated in the inset of Fig. 7, the PL emission intensity initially increased with increasing the Eu^{3+} ion concentration, and then showed a decrement tendency with further raising the activator concentration due to the concentration quenching effect. In order to figure out the involved concentration quenching mechanism, the critical distance (R_c) of Eu^{3+} ions in Gd_2MoO_6 host lattice was estimated by utilizing the Blasse's equation:[42]

$$R_c = 2\left(\frac{3V}{4\pi x_c Z}\right)^{1/3}, \qquad (2)$$

where V stands for the volume of the unit cell, x_c is the critical concentration and Z is the number of cation sites in the unit cell. In this work, the values of V, x_c and Z were 947.65, 0.15 and 8, respectively. Thus, the R_c value was calculated to be around 11.47 Å. As for the nonradiative (NR) ET, which is the main cause of the concentration quenching effect, among the activators, it is usually triggered either by exchange interaction or electric multipole interaction. In general, when the critical distance is smaller than 5 Å, the NR ET is dominated by exchange interaction, otherwise the electric multipole interaction prevails.[43,44] Since the calculated R_c value was much larger than 5 Å, the electric multipole interaction would contribute to the NR ET. According to Dexter's report, the PL emission intensity (I) per doping concentration (x) can be expressed as:[45]

$$\log(I/x) = c - (\theta/3)\log x, \qquad (3)$$

where c is a constant and $\theta = 6$, 8 and 10 stands for dipole–dipole interaction, dipole–quadrupole interaction and quadrupole–quadrupole interaction, respectively. As depicted in Fig. S3,† the relation between $\log(I/x)$ and $\log x$ was linear and the experimental data were fitted with slopes of −1.71 and −1.68 when the excitation wavelength was 360 and 463 nm, respectively. As a consequence, the θ values were determined to be 5.13 and 5.04 which were close to 6, indicating that the dipole–dipole interaction dominated the NR ET among the Eu^{3+} ions in $Gd_2MoO_6:2xEu^{3+}$ phosphors.

To determine the suitable synthetic method for the studied samples, the $Gd_2MoO_6:0.30Eu^{3+}$ phosphors were also prepared by the solid-state reaction method. The PL emission spectra of the $Gd_2MoO_6:0.30Eu^{3+}$ phosphors synthesized by sol–gel and solid-stated reaction routes were illustrated in Fig. S4.† As shown in Fig. S4,† the PL emission intensity of the samples prepared by sol–gel method was much higher in comparison to that of the samples prepared by solid-state reaction method, suggesting that the sol–gel method is more suitable for synthesizing the Eu^{3+}-activated Gd_2MoO_6 phosphors.

3.3 Decay curve and CIE coordinate

The PL decay curves of Eu^{3+}-activated Gd_2MoO_6 phosphors with the optimum doping concentration were examined. As shown in Fig. 8, the decay curves were perfectly fitted by a single exponential decay mode:

$$I = A \exp(-t/\tau) + I_0, \qquad (4)$$

where I_0 and I are the emission intensities at time $t = 0$ and t, respectively, and A is the constant. According to the fitting result, the lifetimes were demonstrated to be about 581 and 537 μs when excited at 360 and 463 nm with the monitoring wavelength of 610 nm, respectively. Based on the PL emission spectra, the Commission International de I'Eclairage (CIE) chromaticity coordinates of the $Gd_2MoO_6:0.30Eu^{3+}$ phosphors were calculated as shown in Fig. 9. Under the excitation of 360 and 463 nm, the color coordinates of the $Gd_2MoO_6:0.30Eu^{3+}$ phosphors were (0.650, 0.350) and (0.653, 0.347), respectively. As depicted in Fig. 9, the color coordinates of the $Gd_2MoO_6:0.30Eu^{3+}$ phosphors approached that of the standard red light (0.670, 0.330). Meanwhile, the calculated CIE coordinates were also comparable with that of the commercial red-emitting phosphor of $Y_2O_2S:Eu^{3+}$ (0.622, 0.351).[46] Furthermore, to better understand the red emission of the Eu^{3+}-activated Gd_2MoO_6 phosphors, the color purity was calculated according to the following expression:[26,47]

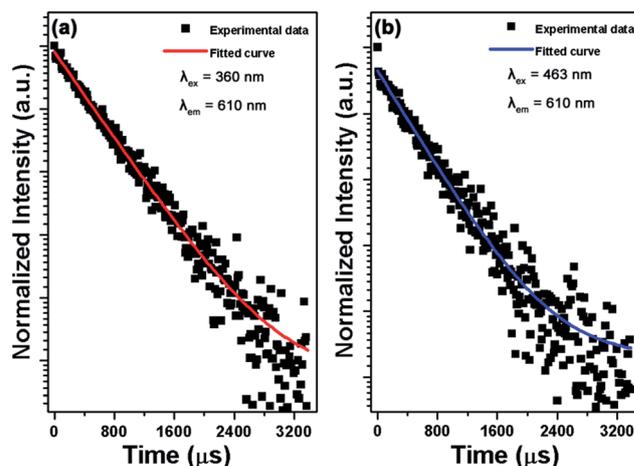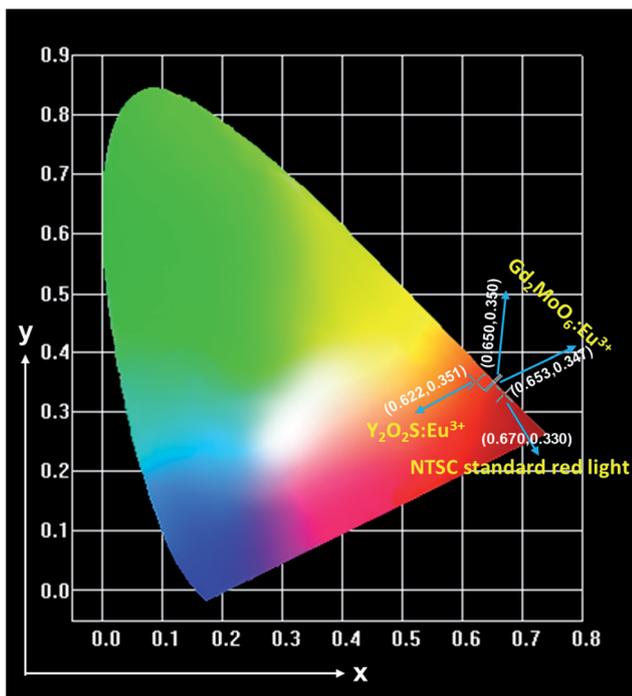**Fig. 8** PL decay curves of the $Gd_2MoO_6:0.30Eu^{3+}$ phosphors under (a) 360 nm and (b) 463 nm excitations.

Fig. 9 CIE chromaticity diagram of the Gd_2MoO_6:0.30Eu^{3+} phosphors, commercial Y_2O_2S:Eu^{3+} phosphor and NTSC standard red light.

$$\text{Color purity} = \frac{\sqrt{(x-x_i)^2 + (y-y_i)^2}}{\sqrt{(x_d - x_i)^2 + (y_d - y_i)^2}}, \quad (5)$$

where (x, y) denotes the CIE coordinate of the synthesized compounds, (x_i, y_i) presents the color coordinate of the white illumination and the (x_d, y_d) is the color coordinate of the dominant wavelength. Here, $(x_d, y_d) = (0.666, 0.334)$ at the dominant wavelength of 610 nm and $(x_i, y_i) = (0.310, 0.316)$. By mean of eqn (5) and the calculated CIE chromaticity coordinates, the color purity for the red emission of the Gd_2MoO_6:0.30Eu^{3+} phosphors was determined to be around 95.8 and 96.6%, respectively, when excited at 360 and 463 nm. These results demonstrated that the Eu^{3+}-activated Gd_2MoO_6 phosphors, which exhibited bright red emission with good CIE chromaticity coordinate and high color purity, may have promising applications in solid-state lighting and display devices as red-emitting phosphors.

3.4 Judd–Ofelt analysis and optical transition parameters

As aforementioned, the Eu^{3+} ions occupied the low symmetry sites with noninversion center in Gd_2MoO_6 host lattice. To get deeper insight into the local structure environment surrounding the Eu^{3+} ions in Gd_2MoO_6 host lattice, the J–O theory was employed to calculate the J–O intensity parameters, that is, Ω_2 and Ω_4. On the basis of J–O theory, the ED spontaneous emission possibility from the initial J state to final J' state can be expressed as:[48,49]

$$A_{ED} = \frac{64\pi^4 e^2}{3h\lambda_{ED}{}^3(2J+1)} \frac{n(n^2+2)^2}{9} \sum_{\lambda=2,4,6} \Omega_\lambda \langle \psi J \| U^\lambda \| \psi' J' \rangle^2, \quad (6)$$

where h is the Plank's coefficient, λ_{ED} is the center wavelength of ED transition, e is the elementary charge, n is the refractive index and $\langle \psi J \| U^\lambda \| \psi' J' \rangle$ refers to the reduced matrix element for the $J \rightarrow J'$ transition. In comparison, the MD spontaneous emission probability from the initial J state to final J' state can be defined as:

$$A_{MD} = \frac{64\pi^4 n^3 S_{md}}{3h\lambda_{MD}{}^3(2J+1)}. \quad (7)$$

In this equation, λ_{MD} is denoted as the center wavelength of MD transition. S_{md} is the MD line strength, which is independent of the luminescent host lattice, and its value is around 7.83×10^{-42}.[50] As is known, the $^5D_0 \rightarrow {}^7F_1$ transition belongs to the MD transition, while the $^5D_0 \rightarrow {}^7F_J$ ($J = 2, 4$) transitions are ED transitions.[51] Therefore, the PL emission intensity ratio (R) between the ED and MD transitions can be expressed as:

$$R = \frac{\int I_{ED} d\lambda}{\int I_{MD} d\lambda}. \quad (8)$$

Combined with eqn (6)–(8), we obtained that

$$\frac{\int I_{ED} d\lambda}{\int I_{MD} d\lambda} = \frac{A_{ED}}{A_{MD}} = \frac{e^2 \lambda_{MD}{}^3}{S_{md}\lambda_{MD}{}^3} \frac{(n^2+2)^2}{9n^2} \sum_{\lambda=2,4,6} \Omega_\lambda \langle \psi J \| U^\lambda \| \psi' J' \rangle^2. \quad (9)$$

For the value of $\int I_{ED} d\lambda / \int I_{MD} d\lambda$, it can be deduced from the integrated area of PL emission spectrum. Since the $^5D_0 \rightarrow {}^7F_6$ transition was not observed in the PL emission spectrum, the Ω_6 can not be evaluated. Meanwhile, the reduced matrix elements are $\langle {}^5D_0 \| U^2 \| {}^7F_2 \rangle^2 = 0.0032$ and $\langle {}^5D_0 \| U^4 \| {}^7F_4 \rangle^2 = 0.0023$.[52] As a consequence, the J–O intensity parameters of Ω_2 and Ω_4 for the Gd_2MoO_6:0.30Eu^{3+} phosphors were calculated to be around 10.18 $\times 10^{-20}$ and 2.82 $\times 10^{-20}$ cm^2, respectively. Note that, the Ω_2 is sensitive to the crystal filed and the large Ω_2 value means low symmetry of the sites of RE ions, while the Ω_4 is related to the bulk performance and the rigidity of the luminescent host lattices.[53] Since the calculated Ω_2 value was much larger than the Ω_4 value, it is rational to consider that the ED transition ($^5D_0 \rightarrow {}^7F_2$) took the domination and the Eu^{3+} ions were located at the low symmetry sites in the Gd_2MoO_6 host lattice, which were in good agreement with the result obtained from the PL emission spectra.

3.5 Thermal stability of the Eu^{3+}-activated Gd_2MoO_6 phosphors

The thermal stability performance of the RE ions activated phosphors is an indispensable parameter for their practical applications in solid-state lighting. The temperature-dependent PL emission spectra for the Gd_2MoO_6:0.30Eu^{3+} phosphors in the temperature range of 303–483 K were recorded. As demonstrated in Fig. 10, the temperature had little effect on the position

of the emission peaks, while the PL emission intensity decreased sharply with the increase of temperature. It is noticeable that the PL emission intensities decreased by 68.9 and 46.9% at 423 K in comparison with that of at room temperature (303 K) when excited at 360 and 463 nm, respectively, as shown in the insets of Fig. 10(a) and (b). The thermal quenching caused by the thermal activation *via* the crossing point between the ground and excited states can be responsible for the fastly deceased PL emission intensity. To determine the activation energy (ΔE), the following expression is given:[54,55]

$$\ln\left(\frac{I_0}{I} - 1\right) = \ln A - \frac{\Delta E}{kT},\qquad(10)$$

where the I_0 stands for the initial PL emission intensity, I is the PL emission intensity at temperature T, A is the constant and k is the Boltzmann constant (8.626×10^{-5} eV K^{-1}). The graphs of $\ln(I_0/I - 1)$ *versus* $1/kT$ were plotted and are depicted in Fig. S5.† It is evident that the experimental data can be linearly fitted with slopes of around −0.417 and −0.383. As a result, the activation energy was determined to be approximately 0.417 and 0.383 eV, respectively, when excited at 360 and 463 nm. This high activation energy suggested that the obtained phosphors possessed good thermal stability and were suitable for WLED applications.
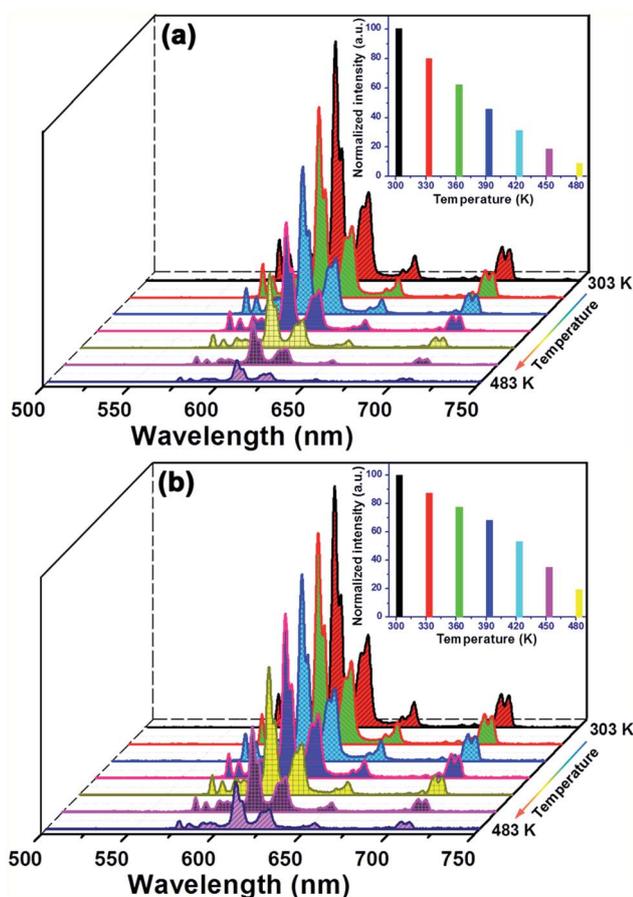
3.6 Quantum efficiency and electroluminescence behavior of fabricated WLED device

Apart from the thermal stability, the quantum efficiency is another vital factor to identify the feasibility of the resultant products for the solid-state lighting applications. The absolute quantum efficiency of the Gd$_2$MoO$_6$:0.30Eu^{3+} phosphors as a function of excitation wavelength was measured. For the Gd$_2$MoO$_6$:0.30Eu^{3+} phosphors, the quantum efficiency was determined to be 26.5 and 47.5% at the excitation wavelengths of 360 and 463 nm, respectively. Clearly, the achieved quantum efficiencies were comparable to those of previous reported red-emitting phosphors, such as Y$_2$O$_2$S:Eu^{3+} and (Ka$_{0.5}$Na$_{0.5}$)NbO$_3$:Eu^{3+}/Bi^{3+},[54,56] further demonstrating that the Eu^{3+}-activated Gd$_2$MoO$_6$ phosphors were promising candidates for WLEDs. As a proof of the above discussion, a WLED device was fabricated by coating the yellow-emitting YAG:Ce^{3+} and red-emitting Gd$_2$MoO$_6$:0.30Eu^{3+} phosphors on the InGaN blue (~456 nm) chip. Meanwhile, for reference, another WLED device, which was made up of InGaN blue chip and yellow-emitting YAG:Ce^{3+} phosphors, was also prepared. The EL spectra of the fabricated WLED devices, which were driven by the forward bias current of 50 mA, were recorded. As disclosed in Fig. S6,† only the emission bands of the blue LED chip and YAG:Ce^{3+} phosphors were detected. However, with the introduction of the resultant red-emitting phosphors, the EL spectrum of the fabricated WLED device could be divided into three parts, namely, the blue emission peak centered at around 456 nm was assigned to the luminescence of blue LED chip, the broad yellow emission band was attributed to the 5d → 4f transition of Ce^{3+} ions in YAG:Ce^{3+} phosphors and the sharp peaks located in the red region belonged to the characteristic emissions of Eu^{3+} ions in the Gd$_2$MoO$_6$:0.30Eu^{3+} phosphors (see Fig. 11). Note that, after adding the Gd$_2$MoO$_6$:0.30Eu^{3+} red-emitting phosphors, the CIR value increased from 70.66 to

Fig. 10 Temperature-dependent PL emission spectra of the Gd$_2$MoO$_6$:0.30Eu^{3+} phosphors under different excitation wavelengths of (a) 360 nm and (b) 463 nm. Inset presents the normalized PL emission intensity as a function of temperature.
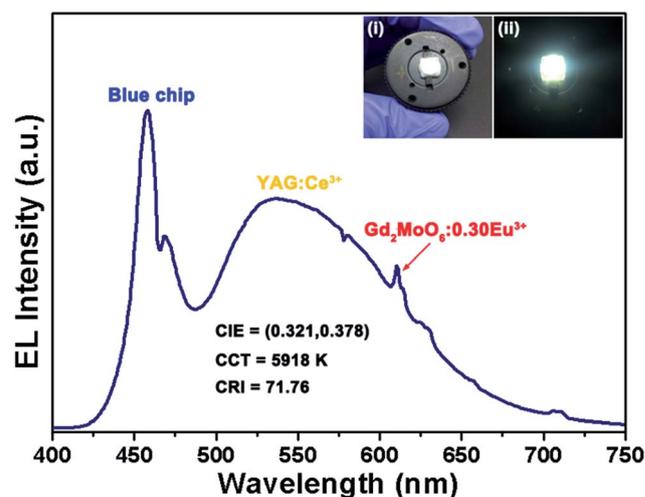

Fig. 11 EL spectrum of the fabricated WLED device by coating the InGaN blue LED chip with commercial yellow-emitting YAG:Ce^{3+} and Gd$_2$MoO$_6$:0.30Eu^{3+} red-emitting phosphors. Inset illustrates the digital images of the fabricated WLED device with and without power input.

71.76, the CCT value decreased from 6124 to 5918 K, and the CIE chromaticity coordinates varied from (0.316, 0.376) to (0.321, 0.378), as depicted in Fig. 11 and S6.† In addition, a red-emitting LED device was also prepared by integrating an InGaN NUV chip with the center wavelength of 375 nm and red-emitting Gd_2MoO_6:0.30Eu^{3+} phosphors. Under forward bias current of 50 mA, the fabricated LED device emitted bright red (0.618, 0.366) light (see the inset of Fig. S7†) and the corresponding EL spectrum consisted of several narrow emission peaks at approximately 577, 589, 610, 655 and 705 nm which were assigned to the featured emissions of Eu^{3+} ions, as presented in Fig. S7.†

4.   Conclusions

In summary, the Gd_2MoO_6:$2x$Eu^{3+} red-emitting phosphors were successfully synthesized and their luminescent properties were analyzed in detail. Under NUV and blue light excitations, the formed compounds exhibited the featured emissions of Eu^{3+} ions and the red emission located at approximately 610 nm ($^5D_0 \rightarrow {}^7F_2$) was dominated in the luminescent spectrum. A gradual enhancement in the PL emission intensity was achieved with the addition of Eu^{3+} ion concentration, exhibiting its maximum value when $x = 0.15$. The critical distance was estimated to be about 11.47 Å and the dipole–dipole interaction should be responsible for the concentration quenching of Eu^{3+} ions in Gd_2MoO_6:$2x$Eu^{3+} phosphors. By means of the J–O theory, the optical transition parameter (Ω_2 and Ω_4) values were increased and the larger Ω_2 value indicated that the Eu^{3+} ions occupied the low symmetry sites in the Gd_2MoO_6 host lattice. Additionally, a WLED device with CCT = 5918 K, CIR = 71.76 and CIE = (0.321, 0.378) was fabricated by integrating the blue LED chip with yellow-emitting YAG:Ce^{3+} and red-emitting Gd_2MoO_6:0.30Eu^{3+} phosphors. From these results, the Eu^{3+}-activated Gd_2MoO_6 phosphors are expected to be very promising in NUV LED-based WLED and blue LED-based WLED applications as red-emitting phosphors.

Acknowledgements

Notes and references

1 J. Shen, Z. Li, R. Cheng, Q. Luo, Y. Chen, X. Chen, Z. Sun and S. Huang, *ACS Appl. Mater. Interfaces*, 2014, **6**, 17454–17462.

2 Z. Yi, X. Li, Z. Xue, X. Liang, W. Lu, H. Peng, H. Liu, S. Zeng and J. Hao, *Adv. Funct. Mater.*, 2015, **25**, 7119–7129.

3 P. Du, L. Luo, H. Park and J. S. Yu, *Chem. Eng. J.*, 2016, **306**, 840–848.

4 M. Wang, *RSC Adv.*, 2016, **6**, 36264–36268.

5 X. Huang, *Nat. Photonics*, 2014, **8**, 748–749.

6 H. Yang, J. Zhang, X. Qin, D. Luo, J. Ma, D. Tang, H. Chen, D. Shen and Q. Zhang, *J. Am. Ceram. Soc.*, 2012, **95**, 52–55.

7 W. Song, W. Di and W. Qin, *Dalton Trans.*, 2016, **45**, 7443–7449.

8 X. Wang, Q. Liu, Y. Bu, C. Liu, T. Liu and X. Yan, *RSC Adv.*, 2015, **5**, 86219–86236.

9 X. Huang, *J. Alloys Compd.*, 2017, **690**, 356–359.

10 C. C. Lin and R. Liu, *J. Phys. Chem. Lett.*, 2011, **2**, 1268–1277.

11 K. Li, H. Lian, M. Shang and J. Lin, *Dalton Trans.*, 2015, **44**, 20542–20550.

12 Y. Liu, Y. Liu, G. Liu, X. Dong and J. Wang, *RSC Adv.*, 2015, **5**, 97995–98003.

13 P. Du, L. K. Bharat and J. S. Yu, *J. Alloys Compd.*, 2015, **633**, 37–41.

14 Z. Xia, Z. Xu, M. Chen and Q. Liu, *Dalton Trans.*, 2016, **46**, 11214–11232.

15 Z. Xia and Q. Liu, *Prog. Mater. Sci.*, 2016, **84**, 59–117.

16 M. Xin, D. Tu, H. Zhu, W. Luo, Z. Liu, P. Huang, R. Li, Y. Cao and X. Chen, *J. Mater. Chem. C*, 2015, **3**, 7286–7293.

17 J. Dhanaraj, R. Jagannathan and D. C. Trivedi, *J. Mater. Chem.*, 2003, **13**, 1778–1782.

18 T. Kuo, W. Liu and T. Chen, *Opt. Express*, 2010, **18**, 8187–8192.

19 S. E. Brinkley, N. Pfaff, K. A. Denault, Z. Zhang, H. T. Hintzen, R. Seshadri, S. Nakamura and S. P. DenBaars, *Appl. Phys. Lett.*, 2011, **99**, 241106.

20 P. Pust, V. Weiler, C. Hecht, A. Tücks, A. S. Wochnik, A. Henβ, D. Wiechert, C. Scheu, P. J. Schmidt and W. Schnick, *Nat. Mater.*, 2014, **13**, 891–896.

21 J. Fu, R. Pang, L. Jiang, Y. Jia, W. Sun, S. Zhang and C. Li, *Dalton Trans.*, 2016, **45**, 13317–13323.

22 J. Zhong, D. Chen, W. Zhao, Y. Zhou, H. Yu, L. Chen and Z. Ji, *J. Mater. Chem. C*, 2015, **3**, 4500–4510.

23 Y. Zheng, H. You, K. Liu, Y. Song, G. Jia, Y. Huang, M. Yang, L. Zhang and G. Ning, *CrystEngComm*, 2011, **13**, 3001–3007.

24 L. Yang, Y. Wan, Y. Huang, C. Chen and H. J. Seo, *J. Alloys Compd.*, 2016, **684**, 40–46.

25 X. Zhang, J. Zhang and M. Gong, *Opt. Mater.*, 2014, **36**, 850–853.

26 P. Du and J. S. Yu, *RSC Adv.*, 2015, **5**, 60121–60127.

27 Z. Zhou, N. Wang, N. Zhou, Z. He, S. Liu, Y. Liu, Z. Tian, Z. Mao and H. T. Hintzen, *J. Phys. D: Appl. Phys.*, 2013, **46**, 035104.

28 L. Wang, H. M. Noh, B. K. Moon, S. H. Park, K. H. Kim, J. Shi and J. H. Jeong, *J. Phys. Chem. C*, 2015, **119**, 15517–15525.

29 H. Jin, H. Wu and L. Tian, *J. Lumin.*, 2012, **132**, 1188–1191.

30 J. Zhang, Y. Liu, L. Li, N. Zhang, L. Zou and S. Gan, *RSC Adv.*, 2015, **5**, 29346–29352.

31 Y. Li and X. Liu, *Mater. Res. Bull.*, 2015, **64**, 88–92.

32 X. Zhang, Y. Chen, S. Zeng and L. Zhou, *Ceram. Int.*, 2014, **40**, 14537–14541.

33 S. Dutta and S. K. Sharma, *J. Mater. Sci.*, 2016, **51**, 6750–6760.

34 L. Jing, X. Liu and Y. Li, *J. Lumin.*, 2015, **158**, 351–355.

35 K. Li, J. Fan, M. Shang, H. Lian and J. Lin, *J. Mater. Chem. C*, 2015, **3**, 9989–9998.

36 X. Min, Z. Huang, M. Fang, Y. Liu, C. Tang and X. Wu, *Inorg. Chem.*, 2014, **53**, 6060–6065.

37 D. Wen, J. Feng, J. Li, J. Shi, M. Wu and Q. Su, *J. Mater. Chem. C*, 2015, **3**, 2107–2114.

38 N. Zhang, C. Guo, J. Zheng, X. Su and J. Zhao, *J. Mater. Chem. C*, 2014, **2**, 3988–3994.

39 Y. Zhang, W. Gong, J. Yu, Y. Lin and G. Ning, *RSC Adv.*, 2015, **5**, 96272.

40 P. Du and J. S. Yu, *Mater. Res. Bull.*, 2015, **70**, 553–558.

41 J. Zhong, D. Chen, Y. Zhou, Z. Wan, M. Ding, W. Bai and Z. Ji, *Dalton Trans.*, 2016, **45**, 4762–4770.

42 G. Blasse, *Philips Res. Rep.*, 1969, **24**, 131–144.

43 S. Som, P. Mitra, V. Kumar, V. Kumar, J. J. Terblans, H. C. Swart and S. K. Sharma, *Dalton Trans.*, 2014, **43**, 9860–9871.

44 N. Zhang, C. Guo, L. Yin, J. Zhang and M. Wu, *J. Alloys Compd.*, 2015, **635**, 66–72.

45 D. L. Dexter, *J. Chem. Phys.*, 1953, **21**, 836–850.

46 Y. Huang and H. J. Seo, *Mater. Lett.*, 2012, **84**, 107–109.

47 V. Mahalingam and J. Thirumalai, *RSC Adv.*, 2016, **6**, 80390–80397.

48 B. R. Judd, *Phys. Rev.*, 1962, **127**, 750–761.

49 G. S. Ofelt, *J. Chem. Phys.*, 1962, **37**, 511–520.

50 L. Wang, W. Guo, Y. Tian, P. Huang, Q. Shi and C. Cui, *Ceram. Int.*, 2016, **42**, 13648–13653.

51 Y. Tian, B. Tian, B. Chen, C. Cui, P. Huang, L. Wang and R. Hua, *J. Alloys Compd.*, 2014, **590**, 61–67.

52 W. T. Carnall, H. Crosswhite and H. M. Crosswhite, *Energy level structure and transition probabilities in the spectra of trivalent lanthanides in lanthanum fluoride*, Argonne National Laboratory Report, 1978.

53 X. Wang, C. Liu, T. Yu and X. Yan, *Phys. Chem. Chem. Phys.*, 2014, **16**, 13440–13446.

54 Q. Zhang, H. Sun, T. Kuang, R. Xing and X. Hao, *RSC Adv.*, 2015, **5**, 4707–4715.

55 Z. Xia, S. Miao, M. S. Molokeev, M. Chen and Q. Liu, *J. Mater. Chem. C*, 2016, **4**, 1336–1344.

56 C. Zhang, H. Liang, S. Zhang, C. Liu, D. Hou, L. Zhou, G. Zhang and Z. Shi, *J. Phys. Chem. C*, 2012, **116**, 15932–15937.